Echoes in unidirectionally rotating molecules

Long Xu,[1,*] Ilia Tutunnikov,[1,*] Lianrong Zhou,[2,*] Kang Lin,[2] Junjie Qiang,[2] Peifen Lu,[2] Yehiam Prior,[1,2,†] Ilya Sh. Averbukh,[1,‡] and Jian Wu[2,3,§]

[1]*AMOS and Department of Chemical and Biological Physics, Weizmann Institute of Science, Rehovot 7610001, Israel*
[2]*State Key Laboratory of Precision Spectroscopy, East China Normal University, Shanghai 200062, China*
[3]*Collaborative Innovation Center of Extreme Optics, Shanxi University, Taiyuan, Shanxi 030006, China*

(Received 16 August 2020; accepted 29 September 2020; published 26 October 2020)

We report the experimental observation of molecular unidirectional rotation (UDR) echoes and analyze their origin and behavior both classically and quantum mechanically. The molecules are excited by two time-delayed polarization-twisted ultrashort laser pulses and the echoes are measured by exploding the molecules and reconstructing their spatial orientation from the detected recoil ions momenta. Unlike alignment echoes which are induced by linearly polarized pulses, here the axial symmetry is broken by the twisted polarization, giving rise to molecular unidirectional rotation. We find that the rotation sense of the echo is governed by the twisting sense of the second pulse even when its intensity is much weaker than the intensity of the first pulse. In our theoretical study, we rely on classical phase-space analysis and on three-dimensional quantum simulations of the laser-driven molecular dynamics. Both approaches nicely reproduce the experimental results. Echoes in general and the unique UDR echoes in particular provide powerful tools for studies of relaxation processes in dense molecular gases.

DOI: 10.1103/PhysRevA.102.043116

I. INTRODUCTION

In 1950, Hahn discovered [1,2] that if an ensemble of spins is irradiated by two properly timed and shaped magnetic field pulses, a spontaneous magnetization of the sample appears at twice the time delay between the two pulses. This response was termed spin echo. This original discovery is a fundamental element in modern nuclear magnetic resonance and magnetic resonance imaging. Various types of echoes have been observed in different nonlinear systems, including photon echoes [3,4], cyclotron echoes [5], plasma-wave echoes [6], cold-atom echoes in optical traps [7–9], and echoes in particle accelerators [10–14]. The concept of echo was extended to single quantum particles and the phenomenon was observed in atoms coupled to a single-mode cavity [15] and in a single vibrationally excited molecule [16].

In the past five years, a new class of molecular alignment and orientation echoes has been discovered and extensively investigated [17–23]. Briefly, a nonresonant optical pulse polarizes the molecules and interacts with the induced dipole, resulting in a torque proportional to $\mathbf{d}_{\rm ind} \times \mathbf{E}$, where $\mathbf{d}_{\rm ind}$ is the dipole moment induced by the electric field $\mathbf{E}$ of the pulse. When a pulse is short compared to the typical molecular rotational period, it impulsively kicks the molecules such that shortly after the pulse, the molecules are aligned along a direction defined by the field polarization (for reviews of molecular alignment see Refs. [24–28]). With time, molecules with different angular velocities step out of phase and the alignment disappears. However, in a manner similar to the original spin echoes, it was shown (see, e.g., [17,19]) that if the molecules are kicked again by a second delayed laser pulse, a spontaneous alignment response emerges at twice the delay between the pulses. Echoes of this type have been used in studies of molecular relaxation in condensed gases [29–32].

Molecules kicked by linearly polarized pulses are equally likely to rotate clockwise or counterclockwise; hence after averaging all molecules, there is no preferred sense of molecular rotation and the ensemble-averaged angular momentum remains zero. Besides linearly polarized pulses, polarization-shaped pulses have also been used to drive molecular rotation. These include pulses in which the polarization of the electric laser field rotates in a plane during the pulse, termed polarization-twisted pulses. Examples of such pulses include a pair of delayed cross-polarized laser pulses [33–35], a chiral train of ultrashort pulses [36,37], polarization-shaped pulses [38–42], and the optical centrifuge for molecules [43–47]. While these pulses are all different, in all cases the field polarization twists in a plane perpendicular to the propagation direction and the timescale of the polarization twisting is comparable to that of the molecular rotation. This allows the molecules to follow the twisting polarization, resulting in molecular unidirectional rotation (UDR) and a nonzero ensemble-averaged angular momentum perpendicular to the plane of polarization twisting. It is not surprising that the dynamics induced by polarization-twisted pulses is different from the alignment dynamics induced by linearly polarized pulses.

*These authors contributed equally to this work.
†yehiam.prior@weizmann.ac.il
‡ilya.averbukh@weizmann.ac.il
§jwu@phy.ecnu.edu.cn

In this paper we report the experimental observation of molecular UDR echo of linear molecules excited by polarization-twisted pulses and provide a detailed theoretical analysis of this effect. In our experiments, the UDR echoes are induced by a pair of corotating or counterrotating delayed polarization-twisted pulses. Each pulse induces molecular UDR, i.e., molecules come to alignment and while being aligned rotate together for a short period of time. At twice the delay between the pulses, molecular UDR spontaneously reoccurs. This recurrence is what we call UDR echo.

One of the techniques for creating a polarization-twisted pulse is by partially temporally overlapping two delayed orthogonally polarized femtosecond laser pulses. The polarization of the resulting laser field rotates continuously from the direction of polarization of the first pulse to that of the second one, thus performing a quarter rotation in a plane [38–41]. The molecular dynamics is followed by using the detection methodology of cold target recoil ion momentum spectroscopy (COLTRIMS) [48,49]. In this technique, an intense probe pulse comes at a variable delay after the pump pulses and Coulomb explodes the molecules. The charged molecular fragments are then guided to a coincidence ion detector, allowing the recording of the three-dimensional (3D) momenta of the particles. Based on this information, the molecular angular distribution at the moment of the Coulomb explosion can be reconstructed.

The present work introduces several elements different from previous works on molecular alignment or orientation echoes. First, in the case of excitation by polarization-twisted pulses, the system lacks axial symmetry and its full characterization involves two degrees of freedom: polar and azimuthal angles. The COLTRIMS detection scheme provides the full angular information and allows us to observe the echo response in both degrees of freedom. Second, the echo observed here is of a different type. During the echo, the molecules not only come to alignment, but the alignment direction rotates with a preferred sense. Perhaps the most surprising observation is that the second polarization-twisted pulse controls the sense of the rotation of the echo. This is unexpected, since the second pulse is less intense and does not change the sign of the ensemble-averaged angular momentum defined by the first polarization-twisted pulse.

The paper is organized as follows. In Sec. II we consider a simplified classical model in which the molecular rotation is restricted to a plane and we discuss the UDR echo from several points of view. Sections III A and III B summarize our experimental and numerical methods, respectively. In Sec. IV we present the experimental results and compare them with the results of three-dimensional classical and quantum simulations. The discussion in Sec. V summarizes the paper.

II. CLASSICAL PERSPECTIVE

A. Introduction to molecular UDR echo

Consider a simplified classical model in which the molecules are rigid and do not interact with each other. The laser pulses propagate along the X axis and the molecules are restricted to rotate in the YZ plane. The carrier frequency of an optical laser pulse is of the order of 10^{15} Hz, while the typical rotational frequency of small molecules is about $h/I \propto 10^{12}$ Hz, where h is Planck's constant and I is the moment of inertia. Therefore, the molecule does not respond to the rapid oscillations of the electric field, allowing averaging of the interaction energy over the optical cycle. The interaction potential due to the laser electric field (averaged over the optical cycle) is given by $V(\psi,t) = -(\Delta\alpha/4)E^2(t)\cos^2(\psi)$ [50–52]. Here ψ is the angle between the molecular axis and the field polarization direction, $\Delta\alpha$ is the molecular polarizability anisotropy, and $E(t)$ is the slowly varying envelope of the laser pulse. We define an additional angle ϕ, the angle between the molecular and Y axes. The equation of motion for ϕ is given by

$$\frac{d^2\phi(t)}{dt^2} = -\frac{1}{I}\frac{dV}{d\psi} = -\frac{\Delta\alpha E^2(t)}{4I}\sin[2\phi(t) - 2\chi(t)], \quad (1)$$

where $\chi = \phi - \psi$ is the angle between the field polarization direction and the Y axis.

To simulate the behavior of a molecular ensemble, we use the Monte Carlo approach and consider a collection of N molecules. Equation (1) is solved numerically for each molecule. Initially, the angle ϕ is uniformly distributed in the interval $(-\pi,\pi]$, while the distribution of angular velocity $\omega \equiv d\phi/dt$ is given by the Boltzmann distribution $p(\omega_0) \propto \exp(-I\omega_0^2/2k_BT)$, where T is temperature and k_B is the Boltzmann constant. In the present work, both in theoretical analysis and in the experiment, we use N_2O molecules and set the initial rotational temperature to $T = 75$ K. The molecular parameters were computed with the help of the density-functional theory (the CAM-B3LYPultrafine/aug-cc-pVTZ method): $I = 39.786$ amu Å^2 and $\Delta\alpha = 2.794$ Å^3 [53].

A polarization-twisted pulse is modeled as a pair of overlapping orthogonally polarized laser pulses with a delay τ_p between them,

$$\mathbf{E}(t) = E_0[f(t)\mathbf{e}_1 + f(t-\tau_p)\mathbf{e}_2], \quad (2)$$

where E_0 is the electric field peak amplitude and $\mathbf{e}_1$ and $\mathbf{e}_2$ are the unit vectors defining the polarizations of the two pulses and are directed along $\pi/4$ (second quadrant) and $-\pi/4$ (first quadrant) with respect to the Y axis, respectively (see Fig. 1). The envelope of each constituent linearly polarized pulse is given by $f(t) = \exp[-2\ln 2(t/\sigma)^2]$, where σ is the full width at half maximum of the laser pulse intensity profile.

Figure 2 shows the time-dependent angular distribution of a molecular ensemble excited by a pair of time-delayed polarization-twisted laser pulses. The first pulse P_1 is applied at $t = 0$ and the second, less intense, pulse P_2 is applied at $t = 3$ ps. For better visibility, we subtract the averaged, between $t = 1.5$ and 2.5 ps, angular distribution. In the case of Fig. 2(a), both pulses twist in the same clockwise sense [$\mathbf{e}_1 \rightarrow \mathbf{e}_2$ (see Fig. 1)]. During the interaction with both pulses, the molecules primarily align along the Y axis ($\phi = 0$), while the shape of the distribution (higher probability is shown in red) suggests that the molecules align along $\mathbf{e}_1$ ($\phi = \pi/4, -3\pi/4$) and, following the twisting polarization, rotate clockwise towards $\mathbf{e}_2$ ($\phi = -\pi/4, 3\pi/4$). The contributions to the ensemble-averaged angular momentum of the two pulses are accumulated in this case, because P_1 and P_2 twist in the same sense. The echo response emerges at twice the delay

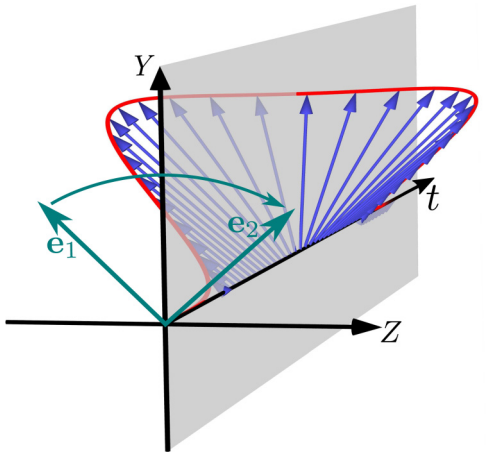

FIG. 1. Illustration of the electric field of the polarization-twisted laser pulse. Here the polarization rotates from the direction defined by $\mathbf{e}_1$ towards the direction of $\mathbf{e}_2$ in a clockwise sense. Both of the vectors $\mathbf{e}_1$ and $\mathbf{e}_2$ are at angle $\pi/4$ with respect to the Y axis.

between P_1 and P_2 (at $t \approx 6$ ps), which is a general feature of the echo phenomenon (see the references in Sec. I). During the echo, molecules transiently align at $\phi = 0, \pi$ and while remaining aligned rotate towards $\phi = \pm\pi/2$. Then, due to the dispersion of molecular angular velocities, the alignment disappears and with it the echo response. After an additional delay of 3 ps (at $t \approx 9$ ps), a second-order echo [13,17–19,42] can be observed (not shown here), and a trace of a third-order echo can be identified at $t \approx 12$ ps (not shown here).

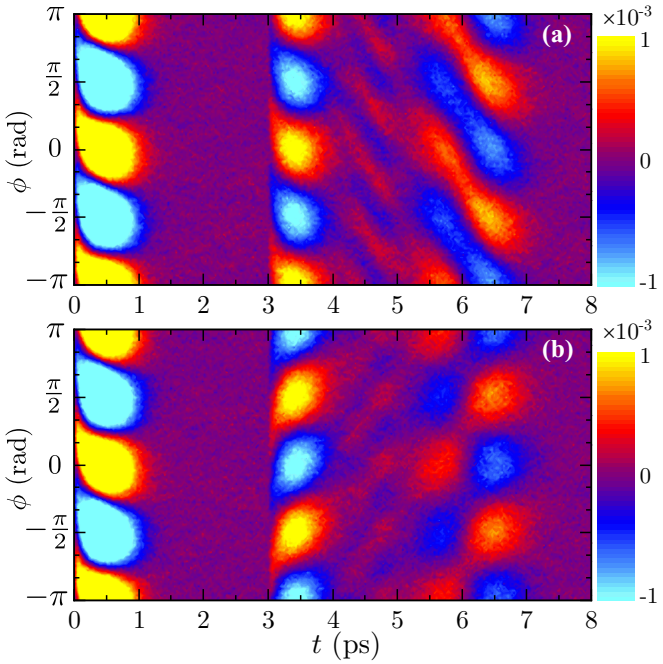

FIG. 2. Time-dependent angular distributions for two cases: (a) Both polarization-twisted pulses P_1 and P_2 twist in the same clockwise sense [$\mathbf{e}_1 \to \mathbf{e}_2$ (see Fig. 1)] and (b) P_1 twists clockwise while P_2 twists counterclockwise ($\mathbf{e}_1 \to -\mathbf{e}_2$). The pulses' parameters are $\sigma = 38$ fs and $\tau_p = 48$ fs [see Eq. (2)]. The peak intensities of P_1 and P_2 are 5.0×10^{13} and 1.9×10^{13} W/cm^2, respectively.

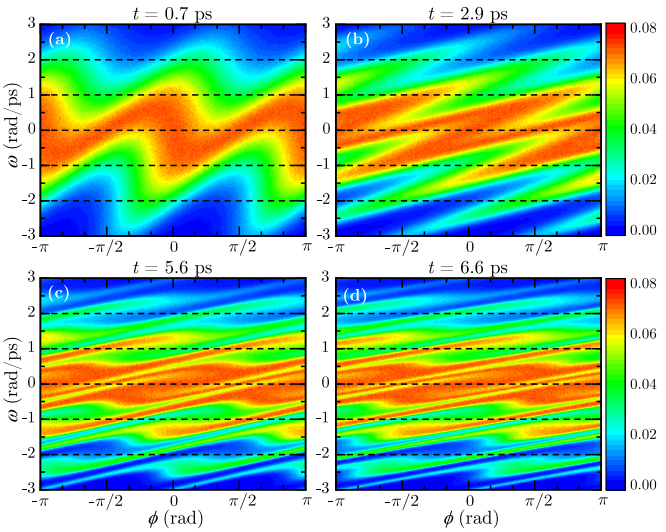

FIG. 3. Phase-space dynamics. Here the polarization-twisted pulses P_1 and P_2 twist in the same clockwise sense [$\mathbf{e}_1 \to \mathbf{e}_2$ (see Fig. 1)] and are applied at $t = 0$ and 3 ps, respectively. The parameters are the same as for the case shown in Fig. 2(a). (a) Shortly after the first pulse. The phase-space distribution shows transient alignment along the Y axis (higher probability near $\phi = 0, \pm\pi$). (b) Filamented phase space just before the second pulse. (c) Moment of alignment echo, with higher probability near $\phi = 0, \pm\pi$, just like after the first pulse. (d) Aligned molecules rotate unidirectionally, resulting in the antialignment phase of the echo (higher probability near $\phi = \pm\pi/2$).

Figure 2(b) shows the echo response for a case when P_1 and P_2 twist in opposite senses: P_1 twists clockwise [$\mathbf{e}_1 \to \mathbf{e}_2$ (see Fig. 1)], inducing a negative ensemble-averaged angular momentum, while P_2 twists counterclockwise [$\mathbf{e}_1 \to -\mathbf{e}_2$ (see Fig. 1)], inducing a positive ensemble-averaged angular momentum. In contrast to the case of corotating pulses [Fig. 2(a)], the contributions of the two pulses to the ensemble-averaged angular momentum are of opposite signs. After the second pulse, the angular momentum remains negative, because the second pulse is not intense enough to cancel the angular momentum introduced by the first pulse. Interestingly, the echo emerging at $t \approx 6$ ps rotates counterclockwise, which is *against* the ensemble-averaged rotation sense of the ensemble [clockwise sense, corresponding to the average negative angular velocity or momentum (see Appendix A)]. In the following sections, we discuss the echo formation mechanism as well as the rotation sense of the molecules forming the echo.

B. Echo formation: Phase-space analysis

Following earlier works [11,17–19], we discuss the echo formation mechanism from the geometrical point of view by considering the phase-space dynamics. Figure 3 shows the phase-space distribution $p(\phi, \omega)$ at different times for the case when both polarization-twisted pulses P_1 and P_2 twist in the same sense [the case shown in Fig. 2(a)]. Figure 3(a) shows that shortly after the first pulse P_1, the molecules come to alignment along the Y axis [higher probability (red) around $\phi = 0, \pi$]. In this sense, a short polarization-twisted pulse

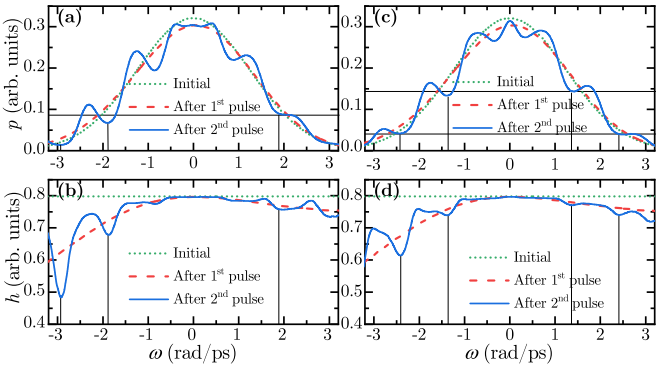

FIG. 4. (a) Distribution of angular velocity $p(\omega)$ and (b) corresponding information entropy $h(\omega)$ for the case shown in Fig. 2(a), where both pulses twist clockwise from $\pi/4$ to $-\pi/4$. (c) and (d) Same as (a) and (b) except that the second pulse twists counterclockwise from $\pi/4$ to $3\pi/4$. The results before the two pulses (initial conditions), after the first pulse, and after the second pulse are shown as dotted green, dashed red, and solid blue lines, respectively.

resembles a pulse with a fixed linear polarization along the Y axis. With time, the phase-space distribution develops multiple parallel filaments [see Fig. 3(b)]. As the number of the filaments grow, they become thinner due to the conservation of the phase-space volume and they form a quasiquantized phase-space pattern [17–19]. Such filamentation of phase space is a known phenomenon in stellar systems [54] and in accelerator physics [55]. In previous works [17–19], it was shown that the phase-space filamentation induced by a single linearly polarized pulse is symmetric with respect to the phase-space origin $(\phi, \omega) = (0, 0)$. As a result, the ensemble-averaged angular velocity or momentum vanishes. Here, in contrast, the polarization-twisted pulse initiates molecular UDR, breaking this symmetry. The total probabilities of finding molecules with positive or negative angular velocity (above or below the horizontal line $\omega = 0$) are unequal (see Appendix A). In other words, the ensemble-averaged angular velocity (momentum) is different from zero.

After the interaction with the second polarization-twisted pulse P_2 (applied at $t = 3$ ps), every filament shown in Fig. 3(b) folds in a manner similar to Fig. 3(a), including the aforementioned asymmetry with respect to the origin. Then, after an additional delay of 3 ps, at $t \approx 6$ ps, the folded parts of the filaments pile up at $\phi = 0, \pi$ [see Fig. 3(c)], representing spontaneous molecular alignment along the Y axis. After the interaction with the second pulse, this recurrence (echo) of the molecular alignment happens due to the quasiquantization [see Fig. 3(b)] of the phase-space distribution. The aligned molecules rotate unidirectionally such that the probability increases near $\phi = \pm\pi/2$ [see Fig. 3(d)].

C. Echo formation: Angular velocity distribution

In this section we take a closer look at the distribution of the angular velocity $p(\omega)$ at different times; $p(\omega)$ is the marginal distribution obtained by integrating the phase-space distribution with respect to the angle ϕ, $p(\omega) = \int_{-\pi}^{\pi} p(\phi, \omega) d\phi$. Figure 4(a) shows the distributions $p(\omega)$ before the application of polarization-twisted pulses, after a single pulse P_1, and after both pulses P_1 and P_2 are applied. Here P_1 and P_2 twist in the same clockwise sense [$\mathbf{e}_1 \rightarrow \mathbf{e}_2$ (see Fig. 1)], similar to Figs. 2(a) and 3. Obviously, the fractions of molecules rotating clockwise and counterclockwise are equal before the pulses. After P_1 (twisting clockwise), there are more molecules rotating clockwise than counterclockwise [$\int_0^{\infty} p(\omega) d\omega < \int_{-\infty}^{0} p(\omega) d\omega$ (see Appendix A)]. Furthermore, since P_2 twists in the same clockwise sense, this imbalance is enhanced after the application of the second pulse. It is evident from Fig. 4(a) that $p(\omega)$ is a slightly asymmetric function of ω. Accordingly, the average angular velocity $\overline{\omega} = \int \omega p(\omega) d\omega$ vanishes before the pulses and is negative after a single pulse P_1 and after the application of both pulses (see Appendix A). In the case of linearly polarized pulses, the distribution $p(\omega)$ always remains symmetric and $\overline{\omega} = 0$. To identify the subgroups of molecules contributing to the echo formation, we use the information entropy [56,57] defined by

$$h(\omega) = -\int_{-\pi}^{\pi} g(\phi, \omega) \log_{10}[g(\phi, \omega)] d\phi, \tag{3}$$

where $g(\phi, \omega) d\phi = p(\phi, \omega) d\phi / p(\omega)$ [$\int_{-\pi}^{\pi} g(\phi, \omega) d\phi = 1$] is the probability of finding a molecule in a small angular interval $d\phi$ around the angle ϕ at angular velocity ω. The information entropy $h(\omega)$ quantifies the similarity between a given distribution and a uniform distribution. Note that the information entropy $h(\omega)$ of a uniform distribution yields the maximum value shown in Figs. 4(b) and 4(d).

Figure 4(b) shows the information entropy for the three distributions presented in Fig. 4(a). Note that the angular velocity remains constant during the stages of free evolution (in the absence of external fields). The initial information entropy is constant (and maximum), as expected for the initially uniform angular distribution. After P_1, the entropy $h(\omega)$ is lower for negative angular velocities. This means that P_1 [twisting clockwise $\mathbf{e}_1 \rightarrow \mathbf{e}_2$ (see Fig. 1)] not only induces molecular UDR, but also increases the angular order of molecules with negative angular velocity. The second polarization-twisted pulse P_2 twists in the same clockwise sense and modulates the distribution of angular velocities [see Fig. 4(a), solid blue curve], which is reflected in the information entropy. Figure 4(b) shows that after P_2, the information entropy develops a series of minima located at $\omega \approx \pm 0.838, \pm 1.885, \pm 2.932$ rad/ps corresponding to subgroups of ordered molecules (their angular distribution differs from the uniform distribution) moving with the characteristic angular velocities.

The contribution to the alignment echo comes mainly from these groups because uniformly distributed molecules do not contribute to the alignment. The difference of angular velocities of the adjacent ordered groups is approximately 1.047 rad/ps, leading to the resynchronization of these groups after $(\pi$ rad$)/(1.047$ rad/ps$) \approx 3$ ps following P_2, in agreement with Figs. 2 and 3.

As an additional example, we consider the case when the second pulse P_2 twists in the opposite sense [counterclockwise $\mathbf{e}_1 \rightarrow -\mathbf{e}_2$ (see Fig. 1)]. Figure 4(c) shows the resulting angular velocity distribution, while Fig. 4(d) shows the corresponding information entropy. In this case,

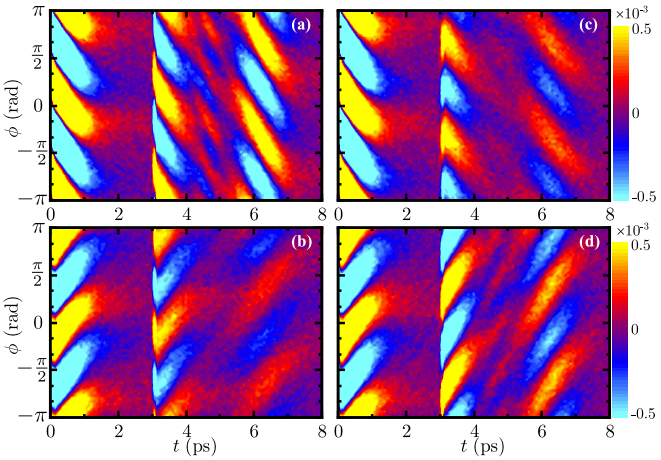

FIG. 5. Time-dependent angular distributions contributed by the molecules with (a) negative and (b) positive angular velocities for the case shown in Fig. 2(a) and (c) negative and (d) positive angular velocities for the case shown in Fig. 2(b).

P_2 competes with P_1 and tends to rotate the molecules in the opposite direction. Here P_1 has higher intensity such that on average (including all molecules) the molecules continue rotating clockwise [after both pulses, $\overline{\omega} < 0$ (see Appendix A)]. The positions of the minima of information entropy in this case are $\omega \approx \pm 0.314, \pm 1.361, \pm 2.408$ rad/ps [see Fig. 4(d)] and are shifted as compared to the minima in the case when both pulses twist in the same sense ($\omega \approx \pm 0.838, \pm 1.885, \pm 2.932$ rad/ps [see Fig. 4(b)]). Besides the shift, the difference of angular velocities between the adjacent minima is the same, 1.047 rad/ps, leading to the echo response after (π rad)/(1.047 rad/ps) $\approx$ 3 ps, like in the first case [see Fig. 2(b)].

D. Effects of the two pulses on the molecular UDR echo

Figure 2 shows that the UDR echo follows the twisting sense of the second polarization-twisted pulse P_2 irrespective of whether it twists in the same or opposite sense relative to the first polarization-twisted pulse P_1. This is counterintuitive since P_2 is less intense and on average the molecules rotate in the sense determined by P_1 (see Appendix A).

Figure 5 shows the angular distributions of molecules with negative and positive angular velocities separately for the two cases shown in Fig. 2. It is evident from Figs. 5(a) and 5(c) that molecules with negative angular velocities come to alignment and collectively rotate clockwise during the echo at $t \approx 6$ ps. Likewise, Figs. 5(b) and 5(d) show that molecules with positive angular velocities come to alignment and rotate counterclockwise during the echo. In addition, Fig. 5 suggests that the second polarization-twisted pulse P_2 enhances the alignment and accelerates the molecules whose sense of rotation matches the sense of polarization twisting of P_2. Having a relatively high alignment factor, these molecules determine the behavior during the echo.

The described molecular UDR echoes are in sharp contrast to the molecular alignment echoes induced by a sequence of linearly polarized pulses [17–19]. In the case of excitation by linearly polarized pulses, the distribution of angular velocities always remains symmetric such that during the echo, the aligned molecules do not rotate with a preferred sense.

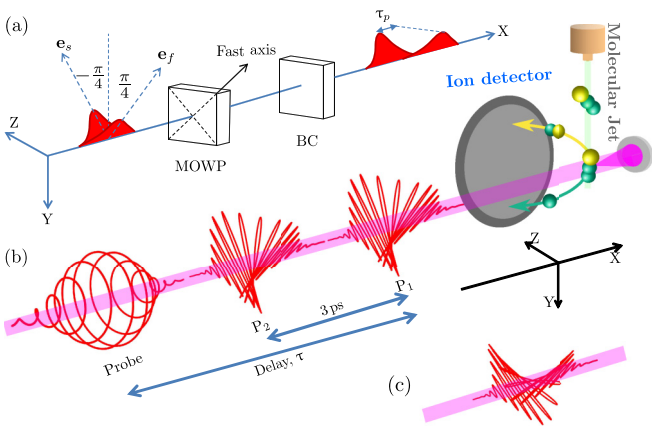

FIG. 6. (a) Optical setup for generating polarization-twisted pulses (see Ref. [40]) described by Eq. (4). A linearly polarized (along the Y axis) pulse propagates along the X axis and passes through a multiple-order waveplate (MOWP) whose fast axis is at $\pi/4$ with respect to the Y axis introducing a delay τ_p (48 fs in our experiment) between the pulse polarization projections (along $\mathbf{e}_f$ and $\mathbf{e}_s$). The pulse continues through a Berek compensator (BC). The introduced delay between the polarization components results in a pulse with polarization twisting from the fast axis $\mathbf{e}_f$ towards the slow axis $\mathbf{e}_s$. (b) Schematic diagram of the experimental setup (see the text). (c) Illustration of the polarization-twisted pulse P_2 used in the second experiment.

III. EXPERIMENTAL AND NUMERICAL METHODS

A. Experimental setup

The measurements were performed in the ultrahigh vacuum chamber of a COLTRIMS apparatus [48,49]. A sequence of laser pulses is focused (by a concave silver mirror with a focal length of $f = 75$ mm) on a supersonic gas jet of N_2O molecules. The laser pulses are produced by a multipass amplifier Ti:sapphire laser system (800 nm, 10 kHz, and 25 fs). In our experiments, we induce molecular UDR using polarization-twisted laser pulses. The pulses are generated following the polarization shaping technique introduced in Ref. [40]. Briefly, a linearly polarized pulse passes through a multiple-order waveplate splitting it into two orthogonally polarized time-delayed (but overlapping) pulses [see the setup in Fig. 6(a)]. The electric field of the resulting laser pulse can be described by [40]

$$\mathbf{E} = E_s(t - \tau_p)\cos(\omega_1 t - \Delta\varphi)\mathbf{e}_s + E_f(t)\cos(\omega_1 t)\mathbf{e}_f, \quad (4)$$

where ω_1 is the central angular frequency, τ_p is the time shift between the cross-polarized pulses which can be adjusted by the multiple-order waveplate, and $\mathbf{e}_s$ and $\mathbf{e}_f$ are the unit vectors along the slow ($-\pi/4$ with respect to the Y axis) and fast ($\pi/4$ with respect to the Y axis) axes, respectively. Here the total relative phase $\Delta\varphi$ is defined by $\Delta\varphi = \omega_1\tau_p + \varphi_p$, where φ_p is the phase difference caused and controlled by a Berek compensator. As depicted in Fig. 6(b), a total of three femtosecond laser pulses are employed in the experiments: polarization-twisted pulses P_1 and P_2 and the circularly

polarized probe pulse. The pulse P_2 follows P_1 with a 3-ps delay and induces the molecular UDR echo after an additional delay of 3 ps. The electric field of both P_1 and P_2 is described by Eq. (4), where the value of $\Delta\varphi$ is set to zero in order to obtain a linear polarization twisting in a plane. For $0 < \Delta\varphi < \pi$, the polarization in the overlap region is elliptical.

An intense circularly polarized probe pulse is sent at a variable delay τ, which Coulomb explodes the N_2O molecules. The ionized fragments, accelerated by a static electric field (approximately equal to 22.3 V/cm), fly towards the position-sensitive microchannel plate detector and time-sensitive delay line detector at one end of the spectrometer. During the off-line analysis, the instantaneous 3D momentum of the fragments during the Coulomb explosion can be reconstructed based on the coincidence measurements. In the experiments, the peak intensities of the pulses P_1 and P_2 and probe pulses are approximately 5.0×10^{13}, 1.9×10^{13}, and 4.0×10^{14} W/cm^2, respectively. The temporal duration of both P_1 and P_2 pulses is approximately 38 fs [see Eq. (4)]. To explore the time-dependent evolution of molecular dynamics, the probe delay (measured from P_1) is scanned from 0 to 49 ps. Since the molecular rotational period is much longer than the timescale of the Coulomb explosion process, the orientation of the molecular axis can be recovered from the reconstructed 3D momentum vectors of the ions. Based on the experimentally measured translation temperature of the molecules [19], the upper limit of the rotational temperature of N_2O molecules in our experiments is estimated to be approximately equal to 75 K.

B. Numerical methods

In what follows, we simulate the echo dynamics under the experimental conditions. For this, we model the laser-driven molecular rotation in three dimensions. Both classical and quantum mechanical formalisms are used and the results are compared to the experiments.

1. Classical simulation

An efficient strategy for simulating the rotational dynamics of an ensemble of rigid bodies relies on the Monte Carlo approach. A sample consisting of N molecules is propagated in time and the appropriate observables are obtained by evaluating the averages over the sample. Generally, the motion of each member of the sample is obtained by solving Euler's equations [58]. The absolute orientation in space is parametrized by quaternions [59,60], which are generalized complex numbers having four components. This approach was used in our previous works [61,62], where the full description of the method is provided. Here we apply the scheme to the linear molecules and model the electric field of the laser pulses by Eq. (2).

2. Quantum simulation

The Hamiltonian describing the rotation of a linear molecule and its interaction with an external field is given by [50–52]

$$\hat{H}(t) = B\hat{J}(\hat{J}+1) + V(t), \tag{5}$$

where $B = \hbar^2/2I$ is the rotational constant and the interaction with the electric field of a nonresonant laser pulse is given by $V(t) = -(\Delta\alpha/4)\sin^2\theta[E_Y(t)\cos(\phi) + E_Z(t)\sin(\phi)]^2$. Here E_Y and E_Z are the envelopes of the field components along the Y and Z axes, respectively, and θ and ϕ are the polar and azimuthal angles of the molecular axis with respect to the laboratory-fixed X and Y axes. The Hamiltonian $\hat{H}$ is expressed in the basis of eigenfunctions $|J, M\rangle$ of the angular momentum operator $\hat{J}$, where J and M are the total angular momentum and its projection on the X axis, respectively. The time-dependent Schrödinger equation $i\hbar\partial_t|\Psi(t)\rangle = \hat{H}(t)|\Psi(t)\rangle$ is solved by numerical exponentiation (see [63]). In addition, the angular distribution $P_{J_0,M_0}(\theta,\phi,t) = |\sum_{J,M} C_{J,M}(t)Y_{J,M}(\theta,\phi)|^2$ is calculated for each initial state $|\Psi(t=0)\rangle = |J_0, M_0\rangle$, where $C_{J,M}(t) = \langle J, M|\Psi(t)\rangle$ is the projection coefficient and $Y_{J,M}(\theta,\phi)$ is the spherical harmonic function. The final probability distribution is obtained by weighted averaging with the Boltzmann weight.

IV. EXPERIMENTAL AND NUMERICAL RESULTS

In our experiments, we use linear N_2O molecules, due to their relatively long revival period $T_{\rm rev} = 39.9$ ps [64] and the absence of 1/4 revival. This provides an extended observation window, of $T_{\rm rev}/2 \approx 20$ ps, for inducing and observing the molecular UDR echo phenomenon. As described in the experimental setup (Sec. III A), molecules are excited by a pair of time-delayed polarization-twisted laser pulses which are followed by a strong circularly polarized probe pulse, inducing Coulomb explosion. Here the double-ionization channel ($N_2O + n\hbar\omega \rightarrow N^+ + NO^+ + 2e^-$) is selected to reproduce the direction of the molecular axis based on the relative momentum between the N^+ and NO^+ fragments originating from the same parent molecule. Using the described pump-probe method, the evolution of the rotational wave packet of N_2O is reconstructed.

Figure 7 shows the time-resolved distribution of azimuthal angle ϕ in the YZ plane (measured with respect to the Y axis). The distribution is normalized at each time step and a background signal is subtracted. The background signal is obtained by averaging the angular distribution over the range of delays between $\tau = 1.5$ and 2.5 ps. As shown in Fig. 6(b), the polarization of P_1 twists clockwise ($\mathbf{e}_f \rightarrow \mathbf{e}_s$, when observed along the negative X axis) from $\pi/4$ to $-\pi/4$ with respect to the Y axis, inducing molecular UDR in the plane of polarization twisting (YZ plane). Accordingly, the angular distribution plotted in Fig. 7(a) exhibits the typical features of molecular UDR, namely, the probability density focuses near $\pi/4$ ($-3\pi/4$) and then moves towards $-\pi/4$ ($3\pi/4$). Due to the dispersion of molecular angular velocities, the angular distribution becomes isotropic once again around $\tau \approx 1.5$ ps. A second, weaker polarization-twisted pulse P_2, twisting in the same sense as P_1, interacts with N_2O at $\tau = 3$ ps, producing an immediate response similar to that following P_1. At twice the delay ($\tau \approx 6$ ps), the molecular UDR echo appears. The echo rotates clockwise, which can be clearly seen in the polar plots for the consecutive probe delays $\tau = 6.05, 6.35, 6.65$ ps shown in Figs. 7(b)–7(d). Numerically calculated angular distributions (both classical and quantum) are in good agreement with the experimental results and display similar molecular

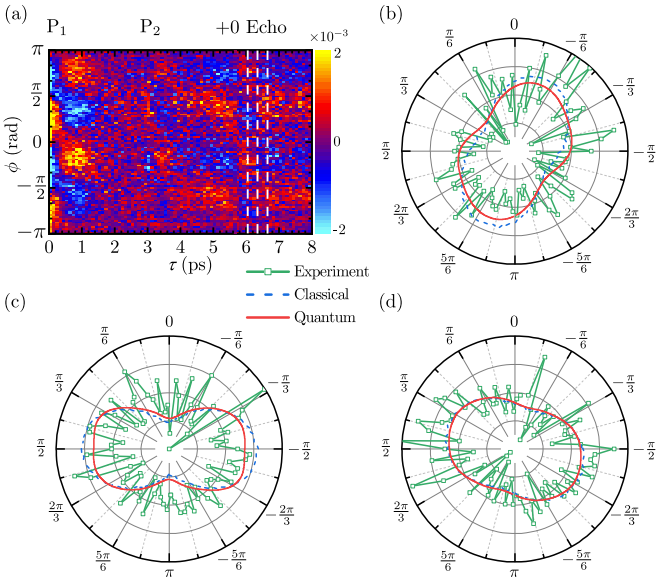

FIG. 7. (a) Experimentally measured time-dependent angular distribution as a function of time for the case when both polarization-twisted pulses $P_{1,2}$ twist in a clockwise sense from $\pi/4$ to $-\pi/4$. Also shown are the polar plots of the experimentally measured (green lines with square markers), simulated classically (dashed blue lines), and quantum mechanically (solid red lines) molecular angular distributions during the UDR echo at (b) $\tau = 6.05$ ps, (c) $\tau = 6.35$ ps, and (d) $\tau = 6.65$ ps.

UDR echo. The clockwise sense of molecular UDR echo is consistent with the twisting direction of the two pulses $P_{1,2}$ and is in agreement with the qualitative picture presented in Sec. II.

We continue with the analysis of long-term behavior and compare it with the results of quantum numerical simulation. As shown in Fig. 8, the half and full revivals induced by the polarization-twisted pulses P_1 and P_2 are marked as $nT_{\rm rev}^{(1)}$ and $nT_{\rm rev}^{(2)}$ ($n = 1/2$ or 1), respectively. In addition, the echo caused by half and full revivals are marked as $+1/2$ Echo and

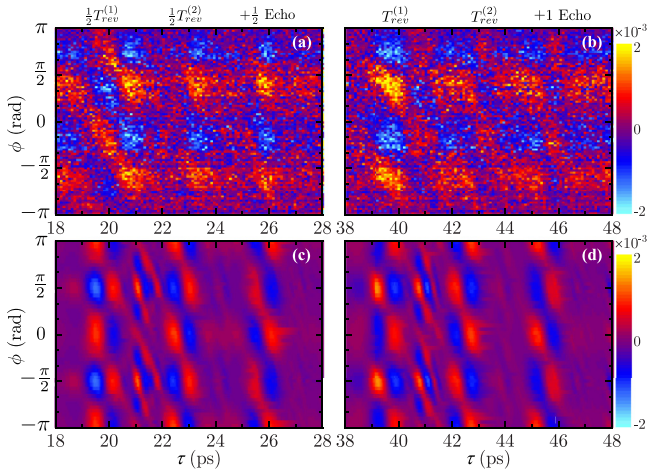

FIG. 8. (a) and (b) Experimentally measured and (c) and (d) calculated (quantum mechanically) time-dependent angular distributions for the case shown in Fig. 7.

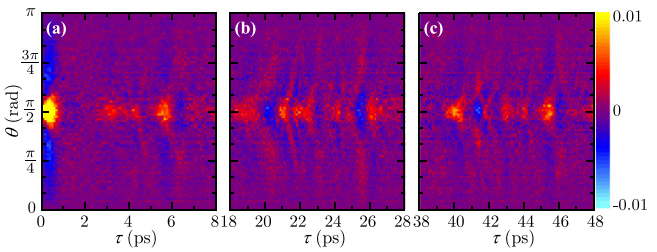

FIG. 9. Experimentally measured time-dependent angular distributions of the polar angle θ for the case shown in Fig. 7.

$+1$ Echo and are visible at $\tau \approx 26$ and 46 ps, respectively. Both the experimental and simulated results show that the molecules coming to alignment during the revival and UDR echo rotate clockwise, which is in the same sense as the twisting of both polarization-twisted pulses P_1 and P_2 and is similar to the behavior observed during the first echo (at $\tau \approx 6$ ps).

Figure 9 reveals a more comprehensive picture of the rotational dynamics. In addition to the distribution of the azimuthal angle ϕ confined to the plane of polarization twisting, we consider the time-dependent angular distribution of the polar angle θ. During the interaction with the polarization-twisted pulses $P_{1,2}$, the N_2O molecules are pulled towards the YZ plane so that the distribution of polar angle θ centers around $\theta = \pi/2$. The same behavior of the polar angle θ is reproduced during the molecular UDR echoes, at $\tau \approx 6, 26, 46$ ps. To summarize, both degrees of freedom θ and ϕ demonstrate the echo phenomenon.

In the first experiment (Fig. 7), the twisting sense of the two polarization-twisted pulses P_1 and P_2 was the same, leading to a molecular UDR echo which rotates in the same sense. In the second experiment, the sense of polarization twisting of P_2 was reversed and it was set to twist counterclockwise from $\phi = \pi/4$ to $3\pi/4$ [see Fig. 6(c)]. The angular distributions at $\tau \approx 6$ ps (around the echo time) show a molecular UDR echo rotating in the counterclockwise sense, from $\pi/4$ ($-3\pi/4$) to $3\pi/4$ ($-\pi/4$), as shown in Fig. 10. In other words, the rotation sense of the UDR echo follows the polarization twisting of the second polarization-twisted pulse P_2. This observation is completely consistent with qualitative analysis presented in Sec. II.

Finally, we would like to point out a slight difference between the results of the classical 2D simulation presented in Fig. 2(b) and the results of the experiment and the 3D simulations presented in Fig. 10. Notice that in Fig. 2(b) at the beginning of the echo event (at $t \approx 5.5$ ps), the molecules come to alignment at $\phi = 0, \pi$, while in Fig. 10 the alignment starts at $\phi = \pm\pi/2$ (just like after the second polarization-twisted pulse). This fine difference between the 2D model and fully three-dimensional classical or quantum simulations is discussed in detail in Appendix B.

V. CONCLUSION

We have reported the observation of molecular UDR echoes. In contrast to previous studies on molecular alignment echoes utilizing linearly polarized pulses, here the

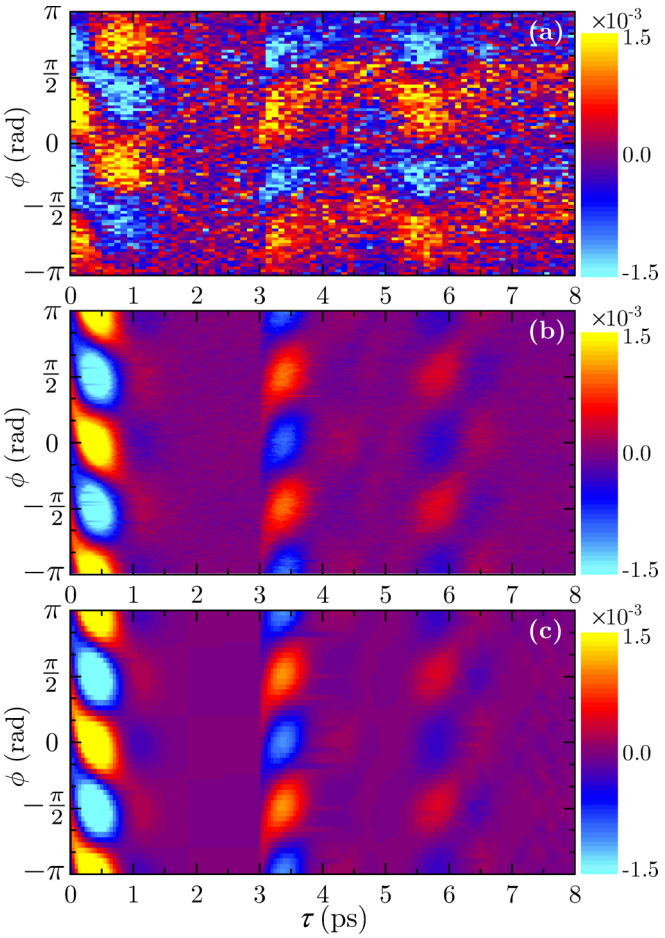

FIG. 10. (a) Experimentally measured angular distribution of the angle ϕ as a function of time. (b) Results of the classical and (c) quantum simulations. The conditions used are the same as the case shown in Fig. 7 except that the polarization-twisted pulse P_2 twists counterclockwise from $\pi/4$ to $3\pi/4$.

polarization-twisted pulses deliver a nonzero average angular momentum to the molecular ensemble. This added angular momentum causes a unique UDR echo dynamics, where the molecules align during the echo and while being aligned also rotate in unison in a preferred sense. We observed experimentally and confirmed theoretically that the sense of the molecular UDR echo can be controlled by choosing the sense of polarization twisting of the second pump pulse P_2. Various excitation strategies involving pulses with twisted polarization may be used to produce the UDR echoes. In particular, an enhanced UDR echo phenomenon is expected when using the optical centrifuge, which is highly efficient in inducing molecular UDR.

For the first measurement of the effect presented here, we utilized the powerful COLTRIMS technique, which provides full spatiotemporal information about the molecular dynamics. In principle, the molecular UDR echoes can also be studied by robust all-optical techniques. For example, a purely optical technique was recently demonstrated [65], allowing one to detect not only the optical birefringence developing during alignment, but also the sense of molecular UDR echo induced by the polarization-twisted pulses.

Since their discovery, molecular rotation echoes were successfully used in studies of molecular relaxation in condensed gases [29–32]. Dense gases of highly excited UDR molecules were shown to exhibit unique collisional dynamics and nontrivial relaxation paths to thermal equilibrium [66–70]. Unidirectional rotation echoes provide complementary information on the relaxation processes, compared to the one offered by the standard rotational echoes generated by parallel linearly polarized pulses. Together, these two kinds of echoes may be used to unravel the relative contributions of various relaxation channels.

ACKNOWLEDGMENTS

This work was supported by the National Key R&D Program of China (Grant No. 2018YFA0306303), the National Natural Science Foundation of China (Grants No. 11834004, No. 61690224, No. 11621404, and No. 11761141004), the 111 Project of China (Grant No. B12024), the Projects from Shanghai Science and Technology Commission (Grant No. 19JC1412200), the Israel Science Foundation (Grant No. 746/15), the ICORE program "Circle of Light," and the ISF-NFSC (Grant No. 2520/17). I.S.A. acknowledges support as the Patricia Elman Bildner Professorial Chair. This research was made possible in part by the historic generosity of the Harold Perlman Family.

APPENDIX A: COMPARING GROUPS OF CLOCKWISE AND COUNTERCLOCKWISE ROTATING MOLECULES

Figure 11 shows the population difference and the average angular velocity of clockwise and counterclockwise rotating

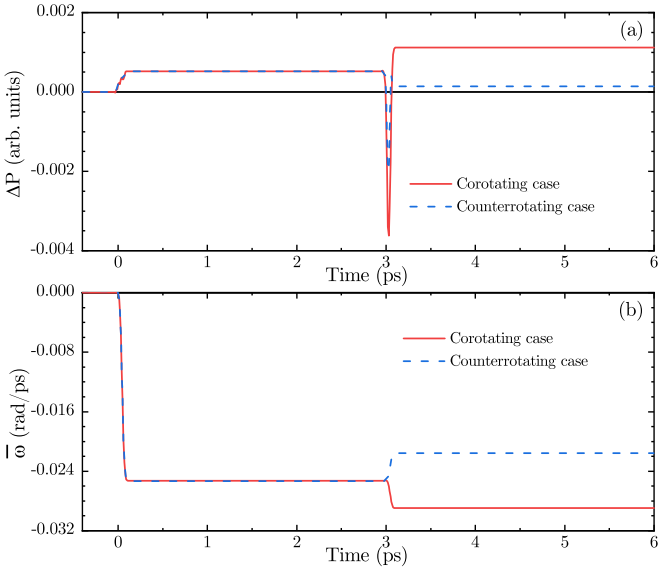

FIG. 11. (a) Time-dependent population difference between molecules with negative and positive angular velocities $\Delta P = \int_{-\infty}^{0} p(\omega)d\omega - \int_{0}^{\infty} p(\omega)d\omega$ and (b) average angular velocity $\overline{\omega} = \int \omega p(\omega)d\omega$ for the two cases shown in Fig. 2. The corotating (solid red lines) and counterrotating cases (dashed blue lines) correspond to the two twisted pulses twisting in the same and opposite directions, respectively.

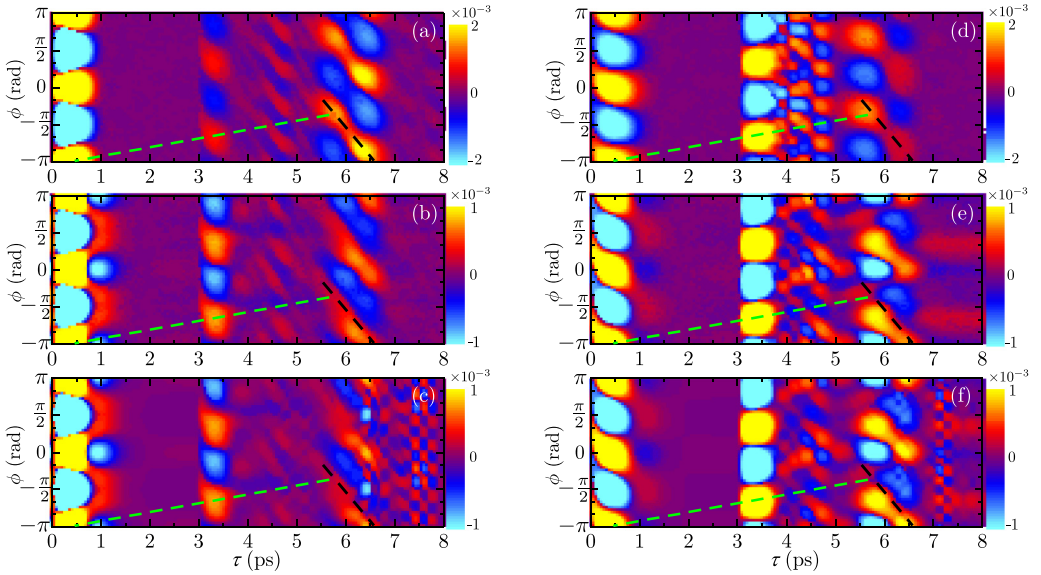

FIG. 12. (a)–(c) Time-dependent angular distributions calculated using (a) the 2D model [Eq. (1)], (b) fully three-dimensional classical simulations, and (c) quantum simulations for the case when a linearly polarized pulse is applied first (P_1) and it is followed by a polarization-twisted pulse (P_2). The pulse parameters are the same as the case shown in Fig. 7. The linearly polarized pulse P_1 is polarized along the Y axis and P_2 twists clockwise from $7\pi/12$ to $\pi/12$. (d)–(f) Time-dependent angular distributions calculated using (d) the 2D model [Eq. (1)], (e) fully three-dimensional classical simulations, and (f) quantum simulations for the case when a polarization-twisted pulse is applied first (P_1) and it is followed by a linearly polarized pulse (P_2). Here P_1 twists clockwise from $\pi/4$ to $-\pi/4$, while P_2 is polarized along $\pi/3$ with respect to the Y axis.

molecules calculated using the 2D model [Eq. (1)]. Before the pulses, the distribution of angular velocities is symmetric. As a result, the populations of molecules with negative and positive angular velocities are equal and the average angular velocity is zero. The polarization direction of the first pulse twists clockwise, leading to a population difference between molecules with negative and positive angular velocities $\triangle P = 0.052\%$ as well as nonzero average angular velocity $\overline{\omega} = -0.0253$ rad/ps. When the second pulse also twists clockwise, the population difference ($\triangle P = 0.112\%$) and the absolute value of the average angular velocity ($\overline{\omega} = -0.0290$ rad/ps) are enhanced. On the other hand, when the second pulse twists in the opposite sense (counterclockwise), the population difference ($\triangle P = 0.014\%$) and the average angular velocity ($\overline{\omega} = -0.0216$ rad/ps) keep the same sign, as after the first pulse (absolute values are decreased). Therefore, in both cases, the molecules rotate on average (including all molecules) clockwise after the application of the two pulses.

APPENDIX B: ANALYSIS OF THE SLIGHT DIFFERENCE BETWEEN THE RESULTS OF 2D AND 3D SIMULATIONS

In this Appendix we consider more closely the difference between the results of the classical 2D simulation presented in Fig. 2(b) and the results of the experiment and 3D simulations presented in Fig. 10. The molecular alignment during the UDR echo obtained using the 2D model is rotated relative to the alignment during the application of the second polarization-twisted pulse. Similar rotated echoes were observed in [20], where two linearly polarized pump pulses were used to induce alignment echoes. The pulses were polarized at different angles and the alignment echo appeared rotated by twice the relative angle between the pulses. To check this and further analyze the difference between the results of 2D and 3D simulations, we substitute one of the polarization-twisted pulses by a linearly polarized pulse.

Figure 12 shows the angular distributions obtained using the 2D model [Eq. (1)] and fully three-dimensional classical simulations, and quantum simulations. Results for two cases are presented: In Figs. 12(a)–12(c) the first pulse is linearly polarized along the Y axis while the second pulse is polarization twisted and in Figs. 12(d)–12(f) the first pulse is polarization twisted while the second pulse is linearly polarized at an angle to the Y axis. The pulses' parameters are the same as in the experiments (see Fig. 7). In both cases, the molecular UDR echo appears at twice the delay between the pulses and it is qualitatively similar. In addition, regardless of whether the polarization-twisted pulse is applied first or second, the molecular UDR echo rotates in the same sense as the polarization twisting.

The results obtained using the 2D model once again differ from the results of 3D simulations. Figures 12(a) and 12(d) show that the location of the initial alignment during the UDR echo is rotated by an additional angle when compared to the results of fully 3D classical and quantum simulations. To summarize, although the 2D model predicts the existence of rotated echo, this prediction is not verified in the more accurate 3D simulations or experiment. Therefore, we conclude that when at least one of the pulses used to induce the UDR echo is polarization twisted, the echo is not rotated.

[1] E. L. Hahn, Spin echoes, Phys. Rev. **80**, 580 (1950).

[2] E. L. Hahn, Free nuclear induction, Phys. Today **6** (11), 4 (1953).

[3] N. A. Kurnit, I. D. Abella, and S. R. Hartmann, Observation of a Photon Echo, Phys. Rev. Lett. **13**, 567 (1964).

[4] S. Mukamel, *Principles of Nonlinear Optical Spectroscopy* (Oxford University Press, Oxford, 1995).

[5] R. M. Hill and D. E. Kaplan, Cyclotron Resonance Echo, Phys. Rev. Lett. **14**, 1062 (1965).

[6] R. W. Gould, T. M. O'Neil, and J. H. Malmberg, Plasma Wave Echo, Phys. Rev. Lett. **19**, 219 (1967).

[7] A. Bulatov, A. Kuklov, B. E. Vugmeister, and H. Rabitz, Echo in optical lattices: Stimulated revival of breathing oscillations, Phys. Rev. A **57**, 3788 (1998).

[8] F. B. J. Buchkremer, R. Dumke, H. Levsen, G. Birkl, and W. Ertmer, Wave Packet Echoes in the Motion of Trapped Atoms, Phys. Rev. Lett. **85**, 3121 (2000).

[9] M. Herrera, T. M. Antonsen, E. Ott, and S. Fishman, Echoes and revival echoes in systems of anharmonically confined atoms, Phys. Rev. A **86**, 023613 (2012).

[10] G. V. Stupakov, Echo effect in hadron colliders, SSC Report No. SSCL-579, 1992, https://doi.org/10.2172/7237216.

[11] G. V. Stupakov and S. K. Kauffmann, Echo effect in accelerators, in *Proceedings of the International Conference on Particle Accelerators, Washington, DC, 1993*, edited by S. T. Corneliussen and L. Carlton (IEEE, Piscataway, 1993), Vol. 1, pp. 197–199.

[12] L. K. Spentzouris, J.-F. Ostiguy, and P. L. Colestock, Direct Measurement of Diffusion Rates in High Energy Synchrotrons using Longitudinal Beam Echoes, Phys. Rev. Lett. **76**, 620 (1996).

[13] G. V. Stupakov, in *Handbook of Accelerator Physics and Engineering*, 2nd ed., edited by A. W. Chao, K. H. Mess, M. Tigner, and F. Zimmermann (World Scientific, Singapore, 2013), Chap. 2.3.13, pp. 121–123.

[14] T. Sen and Y. S. Li, Nonlinear theory of transverse beam echoes, Phys. Rev. Accel. Beams **21**, 021002 (2018).

[15] T. Meunier, S. Gleyzes, P. Maioli, A. Auffeves, G. Nogues, M. Brune, J. M. Raimond, and S. Haroche, Rabi Oscillations Revival Induced by Time Reversal: A Test of Mesoscopic Quantum Coherence, Phys. Rev. Lett. **94**, 010401 (2005).

[16] J. Qiang, I. Tutunnikov, P. Lu, K. Lin, W. Zhang, F. Sun, Y. Silberberg, Y. Prior, I. Sh. Averbukh, and J. Wu, Echo in a single vibrationally excited molecule, Nat. Phys. **16**, 328 (2020).

[17] G. Karras, E. Hertz, F. Billard, B. Lavorel, J.-M. Hartmann, O. Faucher, E. Gershnabel, Y. Prior, and I. Sh. Averbukh, Orientation and Alignment Echoes, Phys. Rev. Lett. **114**, 153601 (2015).

[18] G. Karras, E. Hertz, F. Billard, B. Lavorel, G. Siour, J.-M. Hartmann, O. Faucher, E. Gershnabel, Y. Prior, and I. Sh. Averbukh, Experimental observation of fractional echoes, Phys. Rev. A **94**, 033404 (2016).

[19] K. Lin, P. Lu, J. Ma, X. Gong, Q. Song, Q. Ji, W. Zhang, H. Zeng, J. Wu, G. Karras, G. Siour, J.-M. Hartmann, O. Faucher, E. Gershnabel, Y. Prior, and I. Sh. Averbukh, Echoes in Space and Time, Phys. Rev. X **6**, 041056 (2016).

[20] K. Lin, J. Ma, X. Gong, Q. Song, Q. Ji, W. Zhang, H. Li, P. Lu, H. Li, H. Zeng, J. Wu, J.-M. Hartmann, O. Faucher, E. Gershnabel, Y. Prior, and I. Sh. Averbukh, Rotated echoes of molecular alignment: Fractional, high order and imaginary, Opt. Express **25**, 24917 (2017).

[21] D. Rosenberg, R. Damari, S. Kallush, and S. Fleischer, Rotational echoes: Rephasing of centrifugal distortion in laser-induced molecular alignment, J. Phys. Chem. Lett. **8**, 5128 (2017).

[22] B. Wang, L. He, Y. He, Y. Zhang, R. Shao, P. Lan, and P. Lu, All-optical measurement of high-order fractional molecular echoes by high-order harmonic generation, Opt. Express **27**, 30172 (2019).

[23] K. Lin, I. Tutunnikov, J. Ma, J. Qiang, L. Zhou, O. Faucher, Y. Prior, I. Sh. Averbukh, and J. Wu, Spatiotemporal rotational dynamics of laser-driven molecules, Adv. Photon. **2**, 024002 (2020).

[24] H. Stapelfeldt and T. Seideman, Colloquium: Aligning molecules with strong laser pulses, Rev. Mod. Phys. **75**, 543 (2003).

[25] Y. Ohshima and H. Hasegawa, Coherent rotational excitation by intense nonresonant laser fields, Int. Rev. Phys. Chem. **29**, 619 (2010).

[26] S. Fleischer, Y. Khodorkovsky, E. Gershnabel, Y. Prior, and I. Sh. Averbukh, Molecular alignment induced by ultrashort laser pulses and its impact on molecular motion, Isr. J. Chem. **52**, 414 (2012).

[27] M. Lemeshko, R. V. Krems, J. M. Doyle, and S. Kais, Manipulation of molecules with electromagnetic fields, Mol. Phys. **111**, 1648 (2013).

[28] C. P. Koch, M. Lemeshko, and D. Sugny, Quantum control of molecular rotation, Rev. Mod. Phys. **91**, 035005 (2019).

[29] D. Rosenberg, R. Damari, and S. Fleischer, Echo Spectroscopy in Multilevel Quantum-Mechanical Rotors, Phys. Rev. Lett. **121**, 234101 (2018).

[30] H. Zhang, B. Lavorel, F. Billard, J.-M. Hartmann, E. Hertz, O. Faucher, J. Ma, J. Wu, E. Gershnabel, Y. Prior, and I. Sh. Averbukh, Rotational Echoes as a Tool for Investigating Ultrafast Collisional Dynamics of Molecules, Phys. Rev. Lett. **122**, 193401 (2019).

[31] J. Ma, H. Zhang, B. Lavorel, F. Billard, E. Hertz, J. Wu, C. Boulet, J.-M. Hartmann, and O. Faucher, Observing collisions beyond the secular approximation limit, Nat. Commun. **10**, 5780 (2019).

[32] D. Rosenberg and S. Fleischer, Intrinsic calibration of laser-induced molecular alignment using rotational echoes, Phys. Rev. Res. **2**, 023351 (2020).

[33] S. Fleischer, Y. Khodorkovsky, Y. Prior, and I. Sh. Averbukh, Controlling the sense of molecular rotation, New J. Phys. **11**, 105039 (2009).

[34] K. Kitano, H. Hasegawa, and Y. Ohshima, Ultrafast Angular Momentum Orientation by Linearly Polarized Laser Fields, Phys. Rev. Lett. **103**, 223002 (2009).

[35] Y. Khodorkovsky, K. Kitano, H. Hasegawa, Y. Ohshima, and I. Sh. Averbukh, Controlling the sense of molecular rotation: Classical versus quantum analysis, Phys. Rev. A **83**, 023423 (2011).

[36] S. Zhdanovich, A. A. Milner, C. Bloomquist, J. Floß, I. Sh. Averbukh, J. W. Hepburn, and V. Milner, Control of Molecular Rotation with a Chiral Train of Ultrashort Pulses, Phys. Rev. Lett. **107**, 243004 (2011).

[37] C. Bloomquist, S. Zhdanovich, A. A. Milner, and V. Milner, Directional spinning of molecules with sequences of femtosecond pulses, Phys. Rev. A **86**, 063413 (2012).

[38] Y. Kida, S.-i. Zaitsu, and T. Imasaka, Stimulated rotational Raman scattering by a polarization-modulated femtosecond pulse, Phys. Rev. A **77**, 063802 (2008).

[39] Y. Kida, S.-i. Zaitsu, and T. Imasaka, Coherent molecular rotations induced by a femtosecond pulse consisting of two orthogonally polarized pulses, Phys. Rev. A **80**, 021805(R) (2009).

[40] G. Karras, M. Ndong, E. Hertz, D. Sugny, F. Billard, B. Lavorel, and O. Faucher, Polarization Shaping for Unidirectional Rotational Motion of Molecules, Phys. Rev. Lett. **114**, 103001 (2015).

[41] E. Prost, H. Zhang, E. Hertz, F. Billard, B. Lavorel, P. Bejot, J. Zyss, I. Sh. Averbukh, and O. Faucher, Third-order-harmonic generation in coherently spinning molecules, Phys. Rev. A **96**, 043418 (2017).

[42] K. Mizuse, N. Sakamoto, R. Fujimoto, and Y. Ohshima, Direct imaging of direction-controlled molecular rotational wave packets created by a polarization-skewed double-pulse, Phys. Chem. Chem. Phys. **22**, 10853 (2020).

[43] J. Karczmarek, J. Wright, P. Corkum, and M. Ivanov, Optical Centrifuge for Molecules, Phys. Rev. Lett. **82**, 3420 (1999).

[44] D. M. Villeneuve, S. A. Aseyev, P. Dietrich, M. Spanner, M. Yu. Ivanov, and P. B. Corkum, Forced Molecular Rotation in an Optical Centrifuge, Phys. Rev. Lett. **85**, 542 (2000).

[45] L. Yuan, S. W. Teitelbaum, A. Robinson, and A. S. Mullin, Dynamics of molecules in extreme rotational states, Proc. Natl. Acad. Sci. U.S.A. **108**, 6872 (2011).

[46] A. Korobenko, A. A. Milner, and V. Milner, Direct Observation, Study, and Control of Molecular Superrotors, Phys. Rev. Lett. **112**, 113004 (2014).

[47] A. Korobenko, Control of molecular rotation with an optical centrifuge, J. Phys. B **51**, 203001 (2018).

[48] R. Dörner, V. Mergel, O. Jagutzki, L. Spielberger, J. Ullrich, R. Moshammer, and H. Schmidt-Böcking, Cold target recoil ion momentum spectroscopy: A 'momentum microscope' to view atomic collision dynamics, Phys. Rep. **330**, 95 (2000).

[49] J. Ullrich, R. Moshammer, A. Dorn, R. Dörner, L. Ph. H. Schmidt, and H. Schmidt-Böcking, Recoil-ion and electron momentum spectroscopy: Reaction-microscopes, Rep. Prog. Phys. **66**, 1463 (2003).

[50] R. W. Boyd, *Nonlinear Optics* (Academic, New York, 1992).

[51] B. Friedrich and D. Herschbach, Alignment and Trapping of Molecules in Intense Laser Fields, Phys. Rev. Lett. **74**, 4623 (1995).

[52] B. Friedrich and D. Herschbach, Polarization of molecules induced by intense nonresonant laser fields, J. Phys. Chem. **99**, 15686 (1995).

[53] *NIST Computational Chemistry Comparison and Benchmark Database*, edited by R. D. Johnson III, NIST Standard Reference Database No. 101, Release 20 (NIST, Gaithersburg, 2019).

[54] D. Lynden-Bell, Statistical mechanics of violent relaxation in stellar systems, Mon. Not. R. Astron. Soc. **136**, 101 (1967).

[55] A. J. Lichtenberg, *Phase-Space Dynamics of Particles* (Wiley, New York, 1969).

[56] C. E. Shannon, A mathematical theory of communication, Bell Syst. Tech. J. **27**, 379 (1948).

[57] T. M. Cover and J. A. Thomas, *Elements of Information Theory* (Wiley, New York, 1991).

[58] H. Goldstein, C. Poole, and J. Safko, *Classical Mechanics* (Addison-Wesley, San Francisco, 2002).

[59] E. A. Coutsias and L. Romero, The quaternions with an application to rigid body dynamics, Sandia Tech. Report No. SAND2004-0153, 2004, https://digitalrepository.unm.edu/math_fsp/4/.

[60] J. B. Kuipers, *Quaternions and Rotation Sequences: A Primer with Applications to Orbits, Aerospace and Virtual Reality* (Princeton University Press, Princeton, 1999).

[61] I. Tutunnikov, J. Floß, E. Gershnabel, P. Brumer, and I. Sh. Averbukh, Laser-induced persistent orientation of chiral molecules, Phys. Rev. A **100**, 043406 (2019).

[62] L. Xu, I. Tutunnikov, E. Gershnabel, Y. Prior, and I. Sh. Averbukh, Long-Lasting Molecular Orientation Induced by a Single Terahertz Pulse, Phys. Rev. Lett. **125**, 013201 (2020).

[63] R. B. Sidje, Expokit: A software package for computing matrix exponentials, ACM Trans. Math. Softw. **24**, 130 (1998).

[64] H. Jiang, C. Wu, H. Zhang, H. Jiang, H. Yang, and Q. Gong, Alignment structures of rotational wavepacket created by two strong femtosecond laser pulses, Opt. Express **18**, 8990 (2010).

[65] J. Bert, E. Prost, I. Tutunnikov, P. Béjot, E. Hertz, F. Billard, B. Lavorel, U. Steinitz, I. Sh. Averbukh, and O. Faucher, Optical imaging of coherent molecular rotors, Laser Photon. Rev. **14**, 1900344 (2020).

[66] U. Steinitz, Y. Prior, and I. Sh. Averbukh, Laser-Induced Gas Vortices, Phys. Rev. Lett. **109**, 033001 (2012).

[67] A. A. Milner, A. Korobenko, J. W. Hepburn, and V. Milner, Effects of Ultrafast Molecular Rotation on Collisional Decoherence, Phys. Rev. Lett. **113**, 043005 (2014).

[68] A. A. Milner, A. Korobenko, K. Rezaiezadeh, and V. Milner, From Gyroscopic to Thermal Motion: A Crossover in the Dynamics of Molecular Superrotors, Phys. Rev. X **5**, 031041 (2015).

[69] Y. Khodorkovsky, U. Steinitz, J.-M. Hartmann, and I. Sh. Averbukh, Collisional dynamics in a gas of molecular superrotors, Nat. Commun. **6**, 7791 (2015).

[70] U. Steinitz, Y. Khodorkovsky, J.-M. Hartmann, and I. Sh. Averbukh, Dynamics and hydrodynamics of molecular superrotors, ChemPhysChem **17**, 3795 (2016).